

Superconducting and normal state properties of the layered boride OsB₂

Yogesh Singh, A. Niazi, M. W. Vannette, R. Prozorov, and D. C. Johnston
Ames Laboratory and Department of Physics and Astronomy, Iowa State University, Ames, IA 50014
(Dated: December 2, 2024)

OsB₂ crystallizes in an orthorhombic structure (*Pmmn*) which contains alternate boron and osmium layers stacked along the *c*-axis. The boron layers consist of puckered hexagons as opposed to the flat graphite-like boron layers in MgB₂. OsB₂ is reported to become superconducting below 2.1 K. We report results of the dynamic and static magnetic susceptibility, electrical resistivity, heat capacity and penetration depth measurements on arc-melted polycrystalline samples of OsB₂ to characterize its superconducting and normal state properties. These measurements confirmed that OsB₂ becomes a bulk superconductor below $T_c = 2.1$ K. OsB₂ is thus a rare metal diboride superconductor containing puckered boron layers. Our results indicate that OsB₂ is a weak-coupling Type-II superconductor with an electron-phonon coupling constant $\lambda_{ep} \approx 0.4\text{--}0.5$, a small Ginzburg-Landau parameter $\kappa \sim 2.6$ and an upper critical magnetic field $H_{c2}(0.5\text{ K}) \sim 420$ Oe. The temperature dependence of the superfluid density $n_s(T)$ is consistent with an *s*-wave superconductor with a slightly enhanced zero temperature gap $\Delta(0) = 1.9 k_B T_c$ and a zero temperature London penetration depth $\lambda(0) = 0.37 \mu\text{m}$. The magnetic, transport and thermal properties in the normal state of isostructural and isoelectronic RuB₂, which is reported to become superconducting below 1.6 K, are also reported. In the normal state OsB₂ and RuB₂ are Pauli paramagnetic metals with very similar properties: residual resistivity $\rho_0 = 1.7(2)$ and $1.1(1) \mu\Omega \text{ cm}$; Pauli susceptibility $\chi_P = 3.4(5) \times 10^{-5}$ and $5.22(7) \times 10^{-5} \text{ cm}^3/\text{mol}$; electronic specific heat coefficient $\gamma = 1.90(1)$ and $1.72(3) \text{ mJ/mol K}^2$; low temperature T^3 lattice specific heat coefficient $\beta = 0.031(2)$ and $0.015(1) \text{ mJ/mol K}^4$; and density of states at the Fermi energy $N(\epsilon_F) = 2.21(9)$ and $3.0(2)$ states/(eV f.u.) for OsB₂ and RuB₂, respectively.

I. INTRODUCTION

Since the discovery of superconductivity in MgB₂ at a remarkably high temperature $T_c \approx 39$ K,¹ there has been a renewed interest in the study of metal diborides. Many structurally-related *T*B₂ compounds (*T* = Ti, Zr, Hf, V, Cr, Nb, Ta, Mo) have been investigated in the search for superconductivity,^{2,3,4} some of which had already been studied in the past.⁵

Among all binary diborides with the AlB₂ structure, apart from MgB₂, superconductivity has only been reported for ZrB₂ ($T_c \approx 5.5$ K),³ NbB₂ ($T_c \approx 0.6$ K), Zr_{0.13}Mo_{0.87}B₂ ($T_c \approx 5$ K)⁵ and TaB₂ ($T_c \approx 10$ K)² although there are controversies about superconductivity in ZrB₂, NbB₂ and TaB₂.^{3,4} It has been argued using band structure calculations that in MgB₂, the high T_c is due to the B 2*p* bands at the Fermi energy, and that any chemical, structural or other influence that changes this depresses T_c .⁶ OsB₂ and RuB₂, which form in an orthorhombic structure (*Pmmn*) containing deformed boron sheets instead of a planar boron array as in MgB₂, have also been reported to become superconducting below 2.1 K and 1.6 K, respectively.⁷ Recently the bulk modulus of OsB₂ at ambient and high pressure and its hardness have been studied.⁸ Other physical properties of OsB₂ besides T_c have not yet been reported. Band structure calculations suggest that OsB₂ and RuB₂ are indeed metallic.^{9,10}

For comparison, the structures of MgB₂ and OsB₂ are shown in Fig. 1. While MgB₂ has flat graphite-like sheets of boron separated by a layer of transition metal atoms in a hexagonal close packing arrangement [Fig. 1(a)],¹ the OsB₂ structure has sheets of a deformed two-dimensional

network of corrugated boron hexagons. The boron layers lie between two planar transition metal layers which are offset [Fig. 1(b)].⁹

Herein we report the dynamic and static magnetic susceptibility, specific heat, resistivity and penetration depth studies on OsB₂ to characterize its superconducting and normal state properties. We confirmed that OsB₂ is metallic and becomes superconducting below $T_c = 2.1$ K. Our results indicate that OsB₂ is a weak-coupling superconductor with an electron-phonon coupling constant $\lambda_{ep} \approx 0.4\text{--}0.5$, a small Ginzburg-Landau parameter $\kappa \sim 2.6$ and an upper critical magnetic field $H_{c2}(0.5\text{ K})$ of roughly 420 Oe. We also report measurements on RuB₂ which shows similar normal state properties. The paper is organized as follows. Experimental details are given in Sec. II. The structural results are presented in Sec. III A. The normal state electrical resistivity, magnetic susceptibility and heat capacity data are given in Sec. III B and the superconducting properties are given in Sec. III C. The paper is concluded in Sec. IV.

II. EXPERIMENTAL DETAILS

The binary phase diagram of the Os-B system has recently been investigated in detail and it has been shown that OsB₂ melts congruently at about 1870 °C.¹¹ Polycrystalline samples (~ 1 g) of OsB₂ used in this study were therefore prepared by arc-melting. The two OsB₂ samples for which the properties are reported here were prepared with starting materials of different purity. One sample (sample A) was prepared from Os powder

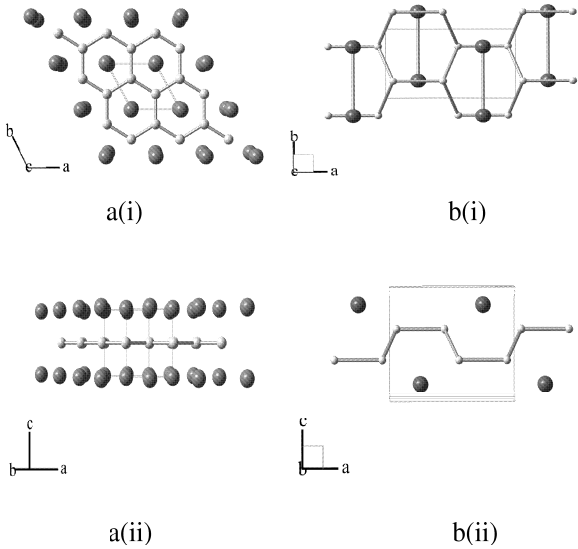


FIG. 1: The crystal structures of MgB_2 (a) and OsB_2 (b). The transition metal atoms are shown as large spheres while the boron atoms are shown as the small spheres. a(i) The MgB_2 structure viewed along the c -axis and a(ii) perpendicular to the c -axis. The MgB_2 structure has alternate boron and transition metals planes stacked along the c -axis. The boron atoms form graphite-like sheets in the ab -plane separated by a layer of transition metal atoms in a hexagonal close packing arrangement.¹ b(i) The OsB_2 structure viewed along the c -axis and b(ii) viewed perpendicular to the c -axis. The OsB_2 structure has a deformed two-dimensional network of corrugated boron hexagon sheets. Along the c -axis the boron layers lie between two planar transition metal layers which are offset along the ab -plane.⁹

(99.95%, Alfa Aesar) and B chunks (99.5%, Alfa Aesar). The magnetization of this sample showed the presence of a large amount of paramagnetic impurities as apparent in the low temperature measurements. Therefore, another sample of OsB_2 (sample B) was prepared using ultrahigh purity Os (99.995%, Sigma Aldrich) and ^{11}B (99.999%, Eagle Pitcher). The magnetization for this sample showed that the concentration of paramagnetic impurities was considerably reduced compared to the first sample. The superconducting transition temperature and transition width are similar for these two samples. Most of the measurements pertaining to the superconducting state have been done on sample A while sample B has been used to obtain the intrinsic magnetic susceptibility of OsB_2 and for ^{11}B NMR measurements which will be reported elsewhere.

The samples were prepared as follows. The constituent elements were taken in stoichiometric proportion and arc-melted on a water-cooled copper hearth in high purity argon atmosphere. A Zr button was used as an oxygen getter. The sample was flipped over and remelted 10-15 times to ensure homogeneous mixing of the constituent elements. The mass of the ingot was checked after the initial two meltings and any weight loss due to the shattering of boron during melting was com-

sated by adding the appropriate amount of boron in subsequent melts. The arc-melted ingot so obtained had a shiny metallic luster with well formed crystal facets on the surface. A sample of the isostructural compound RuB_2 was prepared similarly from high purity Ru powder (99.995%, MV labs) and ^{11}B (99.999%, Eagle Pitcher). A portion of the as-cast samples was crushed for powder X-ray diffraction. Powder X-ray diffraction (XRD) patterns were obtained using a Rigaku Geigerflex diffractometer with $\text{Cu K}\alpha$ radiation, in the 2θ range from 10 to 90° with a 0.02° step size. Intensity data were accumulated for 5 s per step.

Samples of starting composition $\text{OsB}_{1.9}$ and $\text{OsB}_{2.1}$ were also prepared with the above starting materials from Alfa Aesar. Powder X-ray diffraction measurements on crushed pieces of these samples showed that $\text{OsB}_{1.9}$ is a two-phase sample containing the phases Os_2B_3 and OsB_2 while the $\text{OsB}_{2.1}$ sample contained the phase OsB_2 and elemental osmium. The purpose of making these samples was to explore both the boron-deficient and boron-rich sides, respectively, of the homogeneity range of OsB_2 , if any, and its influence on the superconducting properties.

The temperature dependence of the dc magnetic susceptibility and isothermal magnetization was measured using a commercial Superconducting Quantum Interference Device (SQUID) magnetometer (MPMS5, Quantum Design). The resistivity and heat capacity were measured using a commercial Physical Property Measurement System (PPMS, Quantum Design).

The dynamic susceptibility was measured between 0.5 K and 2.5 K using a 10 MHz tunnel-diode driven oscillator (TDO) circuit with a volume susceptibility sensitivity $\Delta\chi \approx 10^{-8}$.¹² For superconductors, this is equivalent to a change in the London penetration depth of about 0.5 Å for millimeter-sized samples.^{12,13,14} A TDO is an LC tank circuit with a coil of inductance L and a capacitor C . The circuit is self-resonating at a frequency $2\pi f = 1/\sqrt{LC}$. When a sample with susceptibility χ is inserted into the coil, the total inductance decreases for a diamagnetic sample or increases for a paramagnetic sample. The resonant frequency changes accordingly by an amount which is proportional to χ .¹² Specifically, the device measures the temperature dependence of the resonant frequency shift $\Delta f(T)$ induced by changes in the sample's magnetic response. The magnetic susceptibility χ is then given by

$$\Delta f(T) = -4\pi\chi(T)G \approx G\Delta\lambda(T), \quad (1)$$

where G is a sample-shape and coil-dependent calibration parameter and $\Delta\lambda = \lambda(T) - \lambda(0) \approx \lambda(T) - \lambda(T_{\min})$ is the change in the London penetration depth $\lambda(T)$ and $T_{\min} = 0.52$ K is the minimum temperature of the measurement. The G has been determined by matching the temperature dependence of the skin depth obtained from the resonator response in the normal state of OsB_2 to the measured resistivity data.

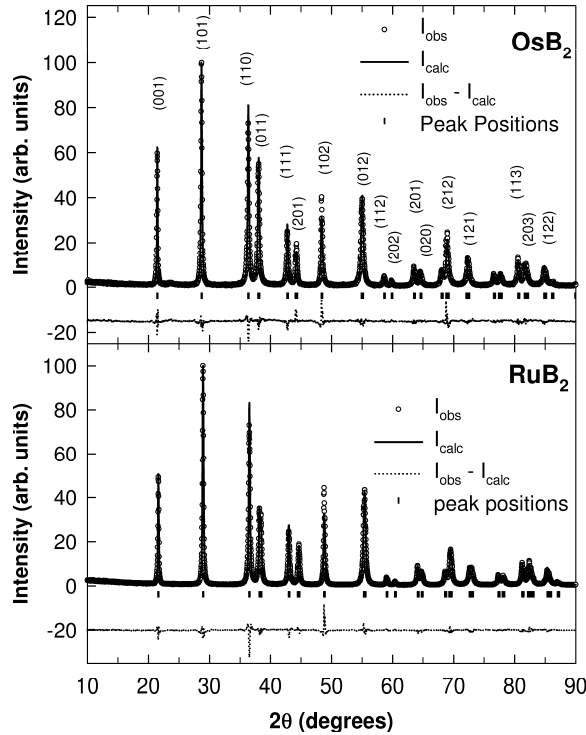


FIG. 2: Rietveld refinements of the OsB_2 and RuB_2 X-ray diffraction data. The open symbols represent the observed X-ray pattern, the solid lines represent the fitted pattern, the dotted lines represent the difference between the observed and calculated intensities and the vertical bars represent the peak positions.

III. RESULTS

A. Structures of OsB_2 and RuB_2

All the lines in the X-ray patterns for OsB_2 and RuB_2 could be indexed to the known orthorhombic $Pmnn$ (No. 59) structure and Rietveld refinements,¹⁵ shown in Fig. 2, of the X-ray patterns gave the lattice parameters: $a = 4.6851(6)$ Å, $b = 2.8734(4)$ Å and $c = 4.0771(5)$ Å for OsB_2 and $a = 4.6457(5)$ Å, $b = 2.8657(3)$ Å and $c = 4.0462(4)$ Å for RuB_2 . These values are in excellent agreement with previously reported values.¹⁶ The best fits were obtained when the anisotropic thermal parameters for the transition metal atom were allowed to vary. For boron the overall isotropic thermal parameter was fixed to zero because unphysically large values were obtained when it was allowed to vary and fixing it to zero did not change the quality of the fit. This is probably because the atomic number of boron is much less than that of either Os or Ru. A neutron diffraction study is needed to obtain reliable estimates of the thermal parameters for boron. Some parameters obtained from the Rietveld refinement are given in Table I. Although the lattice parameters and fractional atomic positions that we obtain from the Rietveld refinements for both OsB_2 and RuB_2

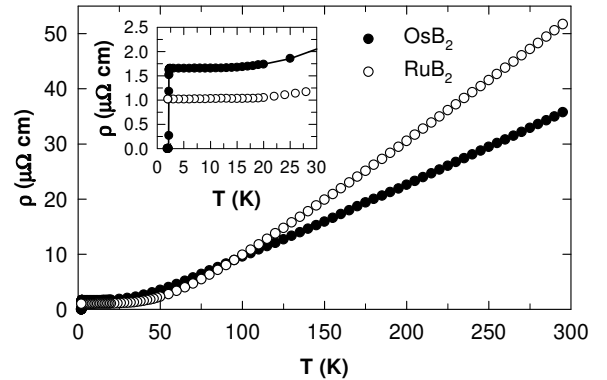


FIG. 3: Electrical resistivity ρ for OsB_2 and RuB_2 versus temperature T . The inset shows the low temperature data on an expanded scale to highlight the low residual resistivity.

agree reasonably well with the earlier structural report,¹⁶ the fits consistently underestimate the intensities of the (102) peaks at $2\theta = 48.35^\circ$ (see Fig. 2).

B. Normal State Properties of OsB_2 and RuB_2

1. Electrical Resistivity

The electrical resistivity (ρ) versus temperature of OsB_2 (sample A) and RuB_2 from 1.75 K to 300 K is shown in Fig. 3. The room temperature resistivity values are $36(3)$ $\mu\Omega$ cm for OsB_2 and $53(5)$ $\mu\Omega$ cm for RuB_2 . The error in the resistivity comes primarily from the error in the determination of the geometrical factors. Both compounds show metallic behavior with an approximately linear decrease in resistivity on cooling from room temperature. At low temperatures ρ becomes only weakly temperature dependent and reaches a residual resistivity ρ_0 of $1.7(2)$ $\mu\Omega$ cm just above 2.2 K for OsB_2 and $1.1(1)$ $\mu\Omega$ cm at 1.8 K for RuB_2 as seen in the inset of Fig. 3. The large residual resistivity ratio $\text{RRR} = \rho(300 \text{ K})/\rho_0 = 22$ for OsB_2 and $\text{RRR} = 51$ for RuB_2 indicates well-crystallized homogenous samples. For OsB_2 the resistivity drops abruptly below 2.2 K and reaches zero by 2.12 K, as highlighted in the inset of Fig. 3. The superconducting properties will be discussed in detail in Sec. III C.

2. Magnetic Susceptibility

Both OsB_2 and RuB_2 are so weakly magnetic that even trace amounts (few ppm) of magnetic impurities are apparent in the low temperature susceptibility and magnetization $M(H)$ measurements. The $M(H)$ data for OsB_2 at 1.8 K, 3.5 K and 5 K are shown in Fig. 4(a). The data

TABLE I: Structure parameters for OsB₂ and RuB₂ refined from powder XRD data. B_{11} , B_{22} and B_{33} are the anisotropic thermal parameters defined within the thermal parameter of the intensity as $e^{-(B_{11}h^2+B_{22}k^2+B_{33}l^2)}$.

Sample	atom	x	y	z	B_{11} (Å ²)	B_{22} (Å ²)	B_{33} (Å ²)	R_{wp}/R_p
OsB ₂	Os	0.25	0.25	0.1515(3)	0.0209(9)	0.045(2)	0.001(1)	1.39
	B	0.093(3)	0.25	0.669(4)				
RuB ₂	Ru	0.25	0.25	0.1490(2)	0.0166(7)	0.051(2)	0.0007(9)	1.36
	B	0.063(1)	0.25	0.638(2)				

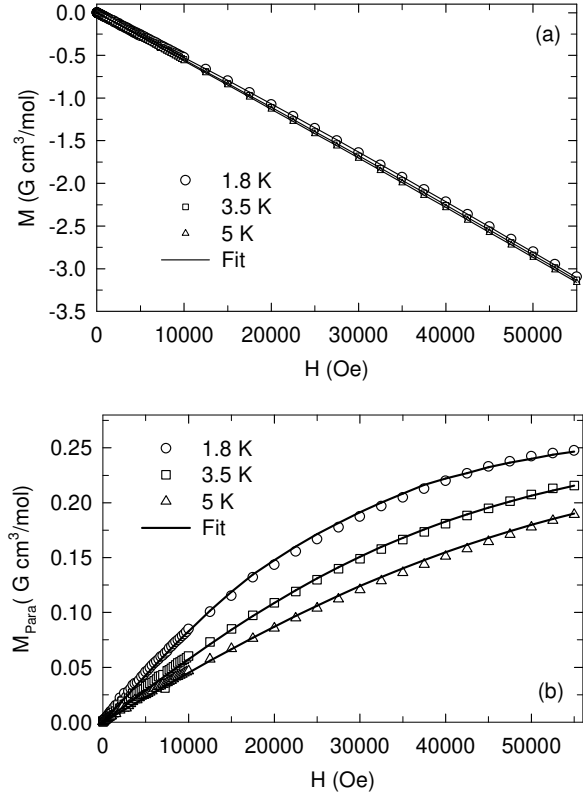


FIG. 4: (a) The magnetization M versus applied magnetic field H for OsB₂. The solid curves are fits by Eq. (2). (b) The paramagnetic impurity contribution M_{Para} to the total $M(H)$. The solid curves are the paramagnetic impurity part of Eq. (2).

were fitted by the expression

$$M(H) = \chi_0 H + f N_A g S \mu_B B_S(x) \equiv \chi_0 H + M_{\text{Para}}(H) , \quad (2)$$

where χ_0 is the intrinsic susceptibility of OsB₂, f is the molar fraction of paramagnetic impurities, N_A is Avogadro's number, g is the g -factor of the impurity spins, S is the spin of the paramagnetic impurities and $B_S(x)$ is the Brillouin function where the argument x of the Brillouin function is $x = g\mu_B S H / (T - \theta)$ where θ is the Weiss temperature. The g value was fixed to two. The fitting parameters were χ_0 , f , S and θ and we obtained: $\chi_0 = -6.09(1) \times 10^{-5} \text{ cm}^3/\text{mol}$, $f = 1.57(4) \times 10^{-5}$,

$S = 1.54(6)$ and $\theta = -1.8(2)$ K. The fit is shown as the solid curves in Fig. 4(a). By subtracting from the observed $M(H)$ data the $\chi_0 H$ obtained from the fitting, one can obtain the contribution from paramagnetic impurities M_{Para} as shown in Fig. 4(b). The solid curves in Fig. 4(b) are the paramagnetic impurity part of the fit [the second term in Eq. (2)].

The normal state susceptibility $\chi \equiv M/H$ for OsB₂ and RuB₂ has been measured versus temperature T between 1.8 K and 300 K in a field of 2 T and 5 T, respectively, as shown in Fig. 5. The $\chi(T)$ for both samples is weakly temperature dependent between 50 K and 300 K. For OsB₂, below 50 K $\chi(T)$ drops slightly on cooling, amounting to about 4% of the room temperature value. The upturn at low temperatures seen for both samples is most likely due to the presence of small amounts (a few ppm) of paramagnetic impurities as determined above for OsB₂ ($f = 16$ molar ppm). Figure 5(a) also shows the susceptibility after subtracting the paramagnetic impurity contribution $\chi_{\text{Para}} = M_{\text{Para}}/H$ from the observed χ .

The intrinsic susceptibility after subtracting χ_{Para} , $\chi(T)$, can be written as

$$\chi = \chi_{\text{core}} + \chi_L + \chi_{\text{VV}} + \chi_P , \quad (3)$$

where χ_{core} is the diamagnetic orbital contribution from the electrons (ionic or atomic), χ_L is the Landau orbital diamagnetism of the conduction electrons, χ_{VV} is the Van Vleck paramagnetic orbital contribution and χ_P is the Pauli paramagnetic spin susceptibility of the conduction electrons. For OsB₂ and RuB₂, the net diamagnetic susceptibility indicates quasi-free electrons with $\chi_L = -(\frac{m}{m^*})^2 \frac{\chi_P}{3}$ and $\chi_{\text{VV}} \approx 0$,¹⁷ where m is the free electron mass and m^* is the effective mass of the current carriers. Assuming $m^* = m$, the Pauli susceptibility can be written as

$$\chi_P = \frac{3}{2}(\chi - \chi_{\text{core}}) , \quad (4)$$

which can be extracted from the experimentally measured susceptibility, after correction for the paramagnetic impurity contribution, if the contribution from the core χ_{core} is known. In covalent metals it is difficult to correctly estimate χ_{core} because its value depends on the local electron density on the atoms. In

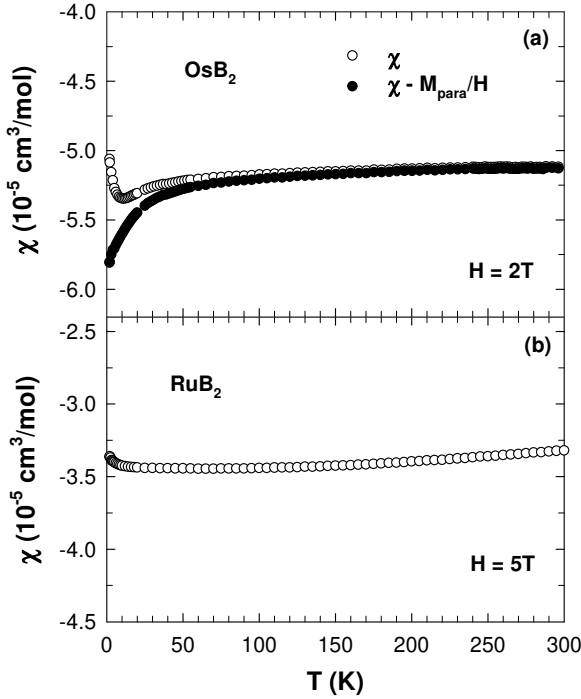


FIG. 5: Magnetic susceptibility χ (open symbols) versus temperature T for OsB_2 (a) and RuB_2 (b). In (a), the filled circles are the values obtained after subtracting the paramagnetic impurity contribution (see text).

an ionic model, $\chi_{\text{core}} = -18 \times 10^{-6} \text{ cm}^3/\text{mol}$ for Os^{6+} and $-44 \times 10^{-6} \text{ cm}^3/\text{mol}$ for Os^{2+} .¹⁸ However if we use the ionic core diamagnetism values for Os and B, one obtains from Eq. (4) an unphysical negative χ_P . For OsB_2 it is reasonable to use atomic (covalent) estimates of χ_{core} instead of ionic values because the bonding in OsB_2 has a strong covalent character.¹⁹ Therefore using the atomic diamagnetism values χ_{core} for Os ($-53.82 \times 10^{-6} \text{ cm}^3/\text{mol}$), Ru ($-42.89 \times 10^{-6} \text{ cm}^3/\text{mol}$) and B ($-12.55 \times 10^{-6} \text{ cm}^3/\text{mol}$),²⁰ we obtain $\chi_{\text{core}} = -78 \times 10^{-6} \text{ cm}^3/\text{mol}$ for OsB_2 and $\chi_{\text{core}} = -68 \times 10^{-6} \text{ cm}^3/\text{mol}$ for RuB_2 . Subtracting these values and the paramagnetic impurity contribution from the total measured susceptibility and accounting for the Landau diamagnetism, one can get the Pauli paramagnetic susceptibility using Eq. (4), thus yielding an average $\chi_P = 3.4(5) \times 10^{-5} \text{ cm}^3/\text{mol}$ for OsB_2 .

From χ_P one can estimate the density of states at the Fermi level $N(\epsilon_F)$ for both spin directions using the relation

$$\chi_P = \mu_B^2 N(\epsilon_F), \quad (5)$$

where μ_B is the Bohr magneton. Taking the above average value of χ_P for OsB_2 , we get $N(\epsilon_F) = 2.2(3) \text{ states}/(\text{eV f.u.})$. This value is somewhat larger than the value from band structure calculations [$N(\epsilon_F) \approx 1.5 \text{ states}/(\text{eV f.u.})$].⁹ Similarly, from the average value of $\chi_P = 5.22(7) \times 10^{-5} \text{ cm}^3/\text{mol}$ for RuB_2 one estimates using Eq. (5), $N(\epsilon_F) = 3.0(2) \text{ states}/(\text{eV f.u.})$.

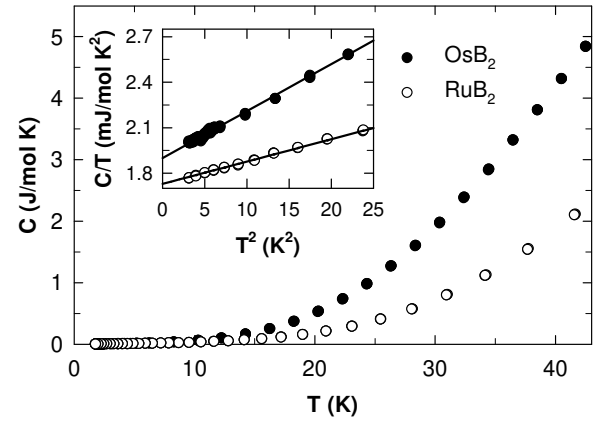


FIG. 6: The heat capacity C versus T of OsB_2 and RuB_2 between 1.8 K and 45 K. The inset shows the data plotted as C/T versus T^2 between 1.8 K and 5 K. The solid lines are fits to the expression $C/T = \gamma + \beta T^2$.

This value is also larger by a factor of 2 than the value obtained from the band structure calculations [$N(\epsilon_F) \approx 1.5 \text{ states}/(\text{eV f.u.})$].⁹

3. Heat Capacity

Figure 6 shows the results of the normal state heat capacity versus temperature $C(T)$ measurements on OsB_2 (sample A) and RuB_2 , plotted as C versus T . The OsB_2 data were recorded in an applied magnetic field of 1 kOe to suppress the superconducting transition to below 1.75 K. The inset in Fig. 6 shows the low temperature data for both samples plotted as C/T versus T^2 . The low temperature data (1.75 K to 5 K) for both samples could be fitted by the expression $C = \gamma T + \beta T^3$ where the first term is the contribution from the conduction electrons and the second term is the contribution from the lattice. The fits are shown as the solid straight lines in the inset of Fig. 6. The values

$$\gamma = 1.90(1) \text{ mJ/mol K}^2 \quad \text{and} \quad \beta = 0.031(2) \text{ mJ/mol K}^4 \quad (6)$$

are obtained for OsB_2 and the values

$$\gamma = 1.72(3) \text{ mJ/mol K}^2 \quad \text{and} \quad \beta = 0.015(1) \text{ mJ/mol K}^4 \quad (7)$$

are obtained for RuB_2 . From the values of β , one can obtain the Debye temperature Θ_D using the expression²¹

$$\Theta_D = \left(\frac{12\pi^4 R n}{5\beta} \right)^{1/3}, \quad (8)$$

where R is the molar gas constant and n is the number of atoms per formula unit ($n = 3$ for OsB_2 and RuB_2). We obtain $\Theta_D = 550(11)$ K for OsB_2 and $\Theta_D = 701(14)$ K for RuB_2 . In a simple harmonic oscillator model $\Theta_D \propto (\frac{1}{M})^{1/2}$ (Ref. 21) where M is the molar

mass of the compound. The ratio $\frac{\Theta_D(OsB_2)}{\Theta_D(RuB_2)} = 0.79(3)$ is indeed close to the square root of the ratio of the molar masses $\sqrt{\frac{M(RuB_2)}{M(OsB_2)}} = 0.76$.

Another quantity which characterizes a metal is the ratio of the density of states as probed by magnetic measurements to the density of states probed by heat capacity measurements, which is the Wilson ratio

$$R_W = \frac{\pi^2 k_B^2}{3\mu_B^2} \left(\frac{\chi_P}{\gamma} \right). \quad (9)$$

For a free-electron Fermi gas $R_W = 1$. Using $\chi_P = 3.4(5) \times 10^{-5} \text{ cm}^3/\text{mol}$ and $\gamma = 1.90(1) \text{ mJ/mol K}^2$ for OsB_2 we get $R_W = 1.3(2)$ which is of the order of unity expected for free electrons. For RuB_2 , $\chi_P = 5.22(7) \times 10^{-5} \text{ cm}^3/\text{mol}$ and $\gamma = 1.72(3) \text{ mJ/mol K}^2$ which gives $R_W = 2.21(7)$.

C. Superconducting Properties of OsB_2

1. Electrical Resistivity and Heat Capacity Measurements

The results of the resistivity $\rho(T)$ and heat capacity $C(T)$ measurements at low temperatures are shown in Fig. 7 to highlight the superconducting transition. Figure 7(a) shows the low temperature resistivity $\rho(T)$ data measured with various applied magnetic fields. In the zero field data there is an abrupt drop below 2.2 K and ρ reaches zero at $T_c = 2.14$ K. The transition is quite sharp with a transition width (10% to 90%) of 60 mK. The superconducting transition is suppressed to lower temperatures in a magnetic field as can be seen in Fig. 7(a). We will return to these data when we estimate the critical field.

Figure 7(b) shows the $C(T)$ data measured in zero and 1 kOe applied field. The sharp anomaly at 2.1 K seen in the heat capacity data taken in zero applied field confirms the bulk nature of the superconductivity in OsB_2 . The transition is completely suppressed to below 1.7 K in 1 kOe as seen in Fig. 7(b). The inset in Fig. 7(b) shows the data plotted as C/T versus T^2 . The jump in the specific heat ΔC at the superconducting transition T_c is usually normalized as $\Delta C/\gamma T_c$ where γ is Sommerfeld's coefficient. Since the anomaly at the superconducting transition is broad and the temperature range below T_c is insufficient, we estimate ΔC by constructing a transition at T_c with a ΔC equal to the maximum of the superconducting anomaly in C/T . This is shown as the solid vertical line in the inset of Fig. 7(b). Using this value of $\Delta C/T_c = 1.78 \text{ mJ/mol K}^2$ and $\gamma = 1.90(1) \text{ mJ/mol K}^2$ obtained in the previous section we get $\Delta C/\gamma T_c = 0.94$. This is reduced from the value 1.43 expected from BCS theory. The origin of this suppression is not currently known. To evaluate this question requires $C(T)$ data to lower temperatures than in Fig. 7(b). However, we reiterate that the large specific heat jump at T_c demonstrates the bulk nature of the superconductivity in OsB_2 .

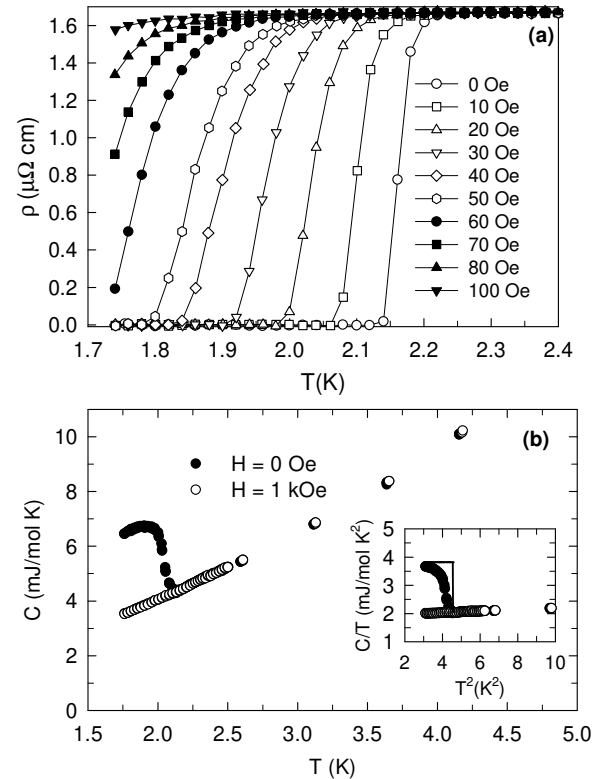


FIG. 7: (a) The resistivity $\rho(T)$ of OsB_2 between 1.7 K and 2.4 K measured with various applied magnetic fields. (b) Temperature dependence of the heat capacity $C(T)$ of OsB_2 in zero and 1 kOe applied magnetic field. The inset shows the data plotted as C/T versus T^2 . The solid line in a construction to estimate the magnitude of the superconducting anomaly. (see text for details)

We now estimate the electron-phonon coupling constant λ_{ep} , using McMillan's formula²² which relates the superconducting transition temperature T_c to λ_{ep} , the Debye temperature Θ_D , and the Coulomb repulsion constant μ^* ,

$$T_c = \frac{\Theta_D}{1.45} \exp\left[-\frac{1.04(1 + \lambda_{\text{ep}})}{\lambda_{\text{ep}} - \mu^*(1 + 0.62\lambda_{\text{ep}})}\right], \quad (10)$$

which can be inverted to give λ_{ep} in terms of T_c , Θ_D and μ^* as

$$\lambda_{\text{ep}} = \frac{1.04 + \mu^* \ln\left(\frac{\Theta_D}{1.45 T_c}\right)}{(1 - 0.62\mu^*) \ln\left(\frac{\Theta_D}{1.45 T_c}\right) - 1.04}. \quad (11)$$

From the heat capacity measurements we had obtained $\Theta_D = 550(11)$ K and using $T_c = 2.1$ K we get $\lambda_{\text{ep}} = 0.41$ and 0.5 for $\mu^* = 0.10$ and 0.15, respectively. These values of λ_{ep} suggest that OsB_2 is a moderate-coupling superconductor (λ_{ep} for MgB_2 is ≈ 1).²³

Having estimated λ_{ep} , the density of states at the Fermi energy for both spin directions $N(\epsilon_F)$ can be estimated from the values of γ and λ_{ep} using the relation²¹

$$\gamma = \frac{\pi^2}{6} k_B^2 N(\epsilon_F)(1 + \lambda_{\text{ep}}) \equiv \gamma_0(1 + \lambda_{\text{ep}}). \quad (12)$$

We find $N(\epsilon_F) = 1.14$ and 1.06 states/(eV f.u.) (f.u. \equiv formula unit) for $\lambda_{ep} = 0.41$ and 0.5 , respectively. These values are comparable with the value estimated by band structure calculations $N(\epsilon_F) \approx 1.5$ (states/eV f.u.).⁹ The bare Sommerfeld coefficient with $\lambda_{ep} = 0.5$ is $\gamma_0 = 1.4$ mJ/mol K².

One can now go back and re-evaluate the Wilson ratio R_W . For a free electron Fermi gas $R_W = 1$. In Sec. III B, using the experimentally observed values of χ_P and γ we had estimated $R_W = 1.5$ for OsB₂. However, the electron-phonon interaction leads to an enhancement in γ from its value γ_0 in the absence of interactions given by $\gamma = \gamma_0(1 + \lambda_{ep})$. Similarly electron-electron interactions lead to an enhancement in the Pauli susceptibility χ_P from its value χ_P^0 in the absence of interactions, given by $\chi_P = \frac{\chi_P^0}{1-\alpha}$, where α is the Stoner enhancement factor. The Wilson ratio is then given by

$$R_W = \frac{\pi^2 k_B^2}{3\mu_B^2} \left(\frac{\chi_P^0}{\gamma_0} \right) = 1 = \frac{\pi^2 k_B^2}{3\mu_B^2} \left(\frac{\chi_P}{\gamma} \right) (1-\alpha)(1+\lambda_{ep}). \quad (13)$$

Using $\lambda_{ep} = 0.5$ and $R_W = 1.3$ obtained in Sec. III B, one gets an estimate of the Stoner enhancement factor $\alpha = 0.49$.

2. dc Magnetization and ac Susceptibility

The temperature dependence of the zero-field-cooled (ZFC) and field-cooled (FC) dimensionless dc volume magnetic susceptibility χ_v of OsB₂ samples A and B in a field of 5 Oe from 1.7 to 2.8 K is plotted in Fig. 8(a), where $\chi_v = M_v/H$ and M_v is the volume magnetization. Complete diamagnetism corresponds to $\chi_v = -1/4\pi$, so the data have been normalized by $1/4\pi$. The data have not been corrected for the demagnetization factor N which gives $\chi_v = \frac{-1/4\pi}{1-N}$ for the measured value. A sharp diamagnetic drop in the susceptibility below $T_c = 2.14$ K for both samples signals the transition into the superconducting state. The width of the transition (10% to 90% of the transition) is 50 mK for sample A and 70 mK for sample B.

In Fig. 8(b) the temperature dependence of the susceptibility of the samples with starting composition OsB_{1.9} and OsB_{2.1} is shown. It can be seen that the onset temperature for the superconducting transition for both the samples is 2.1 K. This indicates that the homogeneity range of OsB₂, if any, does not have any significant effect on the T_c of OsB₂. All other measurements were therefore done on the single phase samples A and B of OsB₂.

To further characterize the superconducting state we have performed measurements of the dc magnetization versus field $M(H)$ at various temperatures and the ac susceptibility (at 10 MHz) versus temperature $\chi(T)$ at various applied magnetic fields. The shape of the $M(H)$ curves in Fig. 9 for OsB₂ are suggestive of Type-I superconductivity with demagnetization effects. However,

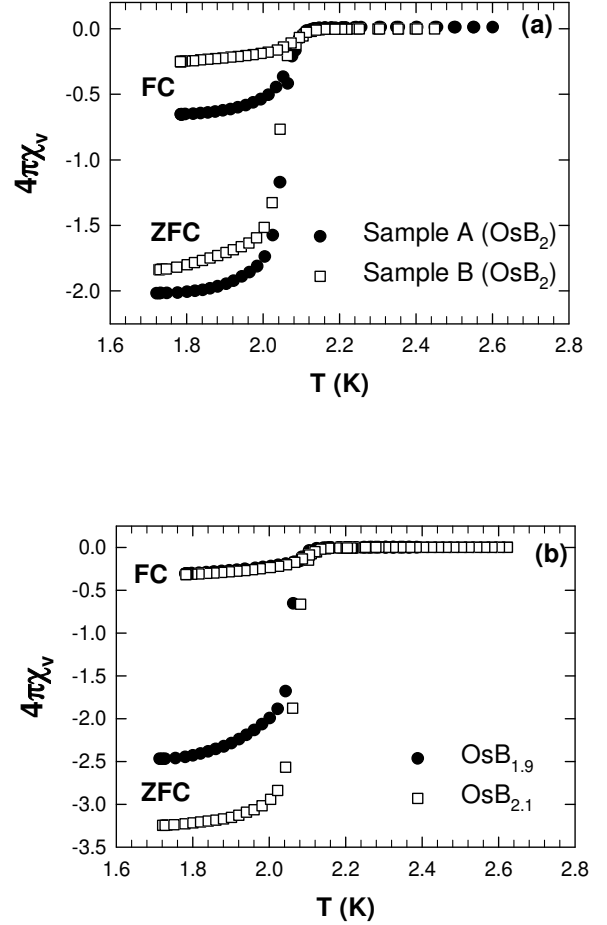


FIG. 8: Temperature T dependence of the zero-field-cooled (ZFC) and field-cooled (FC) volume susceptibility χ_v in terms of the superconducting volume fraction ($4\pi\chi_v$) of OsB₂ (Sample A and Sample B) (a) and OsB_{1.9} and OsB_{2.1} (b) in a field of 5 Oe from 1.7 to 2.4 K.

additional measurements and analysis indicate that OsB₂ is a Type-II superconductor (see below). It will be seen later that the Ginzburg-Landau parameter κ for OsB₂ is small, putting this material on the Type-II side of the derived borderline between Type-I and Type-II and therefore the $M(H)$ in Fig. 9 looks very similar to that for a Type-I superconductor. From the $M(H)$ curves in Fig. 9 we have estimated the critical field $H_{c2}(T)$ from the construction in Fig. 9, illustrated for $T = 1.7$ K. The $H_{c2}(T)$ has been determined by fitting a straight line to the data for a given temperature in the superconducting state and to the data in the normal state and taking the field H at which these lines intersect as the critical field at that temperature $H_{c2}(T)$.

The dynamic ac susceptibility $\chi(T)$ data measured between 0.5 K and 2.2 K in various applied magnetic fields is shown in Fig. 10. To determine $H_{c2}(T)$ from the data in Fig. 10 we have fitted a straight line to the data in the normal state and to the data below T_c for a given applied magnetic field and taken the value of the T at which these lines intersect as the $T_c(H)$. This is shown

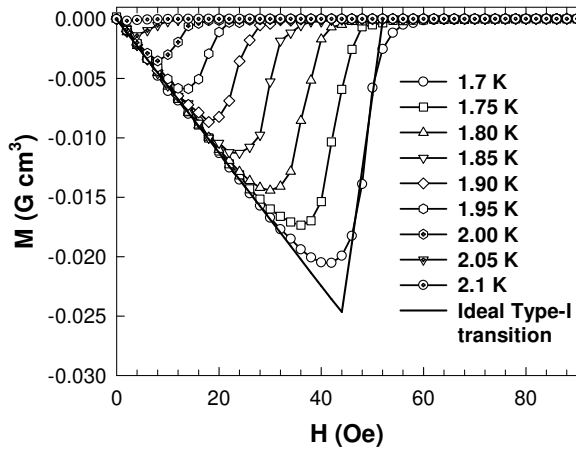


FIG. 9: Magnetization (M) versus applied magnetic field (H) at various temperatures.

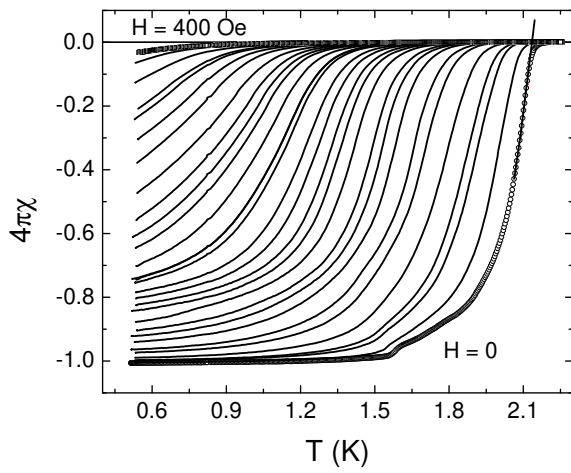


FIG. 10: Dynamic susceptibility χ normalized to $1/4\pi$, versus temperature T with various applied magnetic fields. The data have been normalized to a minimum value of -1 at the lowest T .

in Fig. 10 for the data at $H = 0$. By inverting $T_c(H)$ we obtain $H_{c2}(T)$. The H_{c2} has also been obtained in a similar way from the $\chi(T) \equiv M(T)/H$ SQUID magnetometer data (not shown here) between 1.7 K and 2.4 K in various applied magnetic fields. From the $\rho(T)$ measurements [see Fig. 7(b)] the applied magnetic field has been taken to be the H_{c2} for the temperature at which the resistance drops to zero.

3. Analysis and Discussion of $H_{c2}(T)$ and Superfluid Density

The data for $H_{c2}(T)$ obtained from all the measurements are plotted in Fig. 11. In the temperature range of the SQUID magnetometer measurements (1.7 K to 2.4 K) all the data match well and the temperature dependence of H_{c2} is linear. However, there is an upward

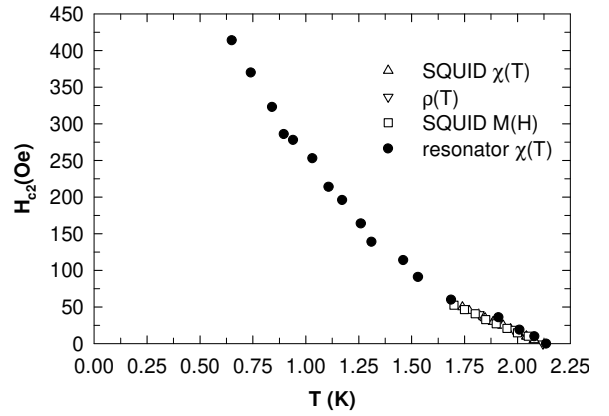


FIG. 11: Upper critical magnetic field H_{c2} versus temperature T extracted from four different types of measurements.

curvature in $H_{c2}(T)$ at lower temperatures as seen in the $H_{c2}(T)$ data extracted from the ac $\chi(T)$ measurements. This upward curvature is not unusual and is often seen in strong coupling superconductors and also in the multi-band superconductor MgB_2 .²⁴ The reason for the positive curvature in $H_{c2}(T)$ for OsB_2 needs to be investigated.

The temperature dependence of the London penetration depth, $\Delta\lambda(T) = \lambda(T) - \lambda(T_{\min}) = \lambda(T) - \lambda(0.52 \text{ K})$, is obtained from the $\chi(T)$ data at $H = 0$ in Fig. 10 using Eq. (1). The result is shown in Fig. 12(a). The temperature dependence of the superfluid density $n_s(T)$ (the fraction of condensed electrons) can be obtained from the London penetration depth λ using the relation²⁵

$$n_s = \frac{1}{\left(1 + \frac{\Delta\lambda(T)}{\lambda(0)}\right)^2}, \quad (14)$$

where here $\Delta\lambda = \lambda(T) - \lambda(0)$. The $n_s(T)$ data thus obtained are shown in Fig. 12(b), where we have set $\lambda(0) = \lambda(0.52 \text{ K})$ when using Eq. (14). Estimates of the value of the zero temperature superconducting gap $\Delta(0)$ and $\lambda(0)$ were obtained by fitting the full temperature range $n_s(T)$ data in Fig. 12(b) by a BCS model using a semi-classical approximation.^{26,27} The fit gave the value $\lambda(0) = 0.39(2) \mu\text{m}$ and a slightly enhanced value for the superconducting gap $\Delta(0) = 1.90(5) k_B T_c$. Figure 12(b) shows the results of the full-temperature BCS calculations for a weak-coupling s -wave BCS model with a gap $\Delta(0) = 1.76 k_B T_c$ (solid curve) and the result for an s -wave BCS model with a gap $\Delta(0) = 1.90(5) k_B T_c$ (dashed curve). The overall behavior is clearly consistent with an s -wave superconductor and the data are consistent with a slightly enhanced gap $\Delta(0) = 1.90(5) k_B T_c$.

We now estimate the Ginzburg-Landau parameter $\kappa = \frac{\lambda(0)}{\xi}$ where ξ is the $T = 0$ coherence length. First, the residual resistivity $\rho_0 = 1.66 \mu\Omega \text{ cm}$ (see inset in Fig. 3) gives the mean free path $l = mv_F/\rho_0 ne^2 = 0.022 \mu\text{m}$, where m is taken to be the free electron mass, v_F is the Fermi velocity, n is the conduction electron density and e is the electron charge. The n was estimated from the

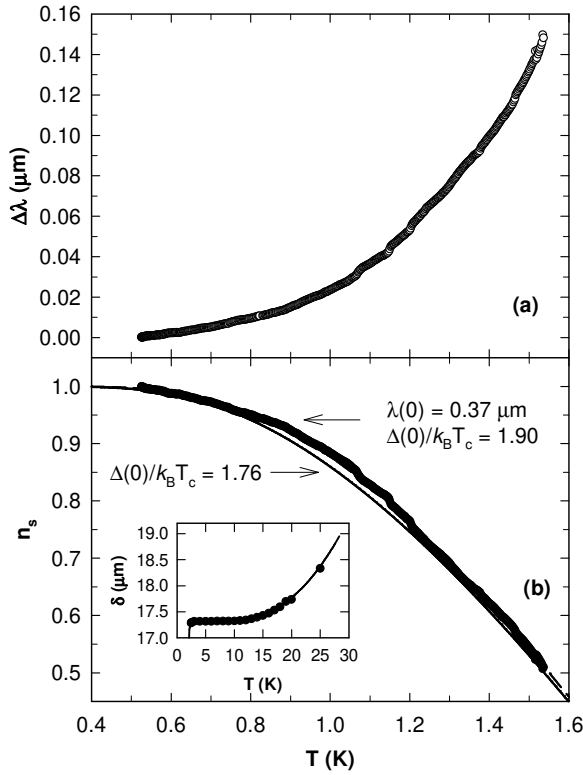


FIG. 12: (a) The temperature T dependence of the change $\Delta\lambda$ in penetration depth in zero magnetic field $\Delta\lambda(T) \equiv \lambda(T) - \lambda(0.52 \text{ K})$. (b) The temperature dependence of the superfluid density $n_s(T)$ of OsB_2 . The solid circles are the data, the dashed line is a fit by the standard s -wave BCS model where the superconducting gap $\Delta(0)$ was allowed to vary and the solid line is a fit by the standard s -wave BCS model with the gap fixed to the weak-coupling BCS value $\Delta(0) = 1.76 \text{ K}_\text{B}T_\text{c}$. The inset shows the calibrated normal-state skin-depth (solid curve) compared to the data from resistivity measurements (solid circles).

electronic specific heat coefficient γ assuming a quasi-free electron model which gives²¹

$$\gamma_0 = \frac{4\pi^4 k_\text{B}^2 m^* N_\text{A}}{h^2 (3\pi^2 n)^{\frac{2}{3}}} . \quad (15)$$

Here, $\gamma_0 = 1.4 \text{ mJ/mol K}^2$ is the above bare electronic specific heat coefficient, k_B is Boltzmann's constant, m^* is the effective mass of the current carriers, N_A is Avogadro's number, and h is Planck's constant. Using Eq. (15), with m^* equal to the free electron mass, we get a very large conduction electron density $n = 20 \times 10^{22} \text{ cm}^{-3}$ resulting²¹ in a $v_\text{F} = (\frac{h}{2\pi m})(3\pi^2 n)^{\frac{2}{3}} \approx 2.1 \times 10^8 \text{ cm/s}$. The BCS coherence length is then²⁸ $\xi_0 = h v_\text{F} / [2\pi^2 \Delta(0)] \simeq 1.26 \mu\text{m}$. Since $\xi_0 \gg l$, OsB_2 is in the dirty limit and the actual coherence length is given

by²⁸ $\xi = 0.85\sqrt{\xi_0 l} = 0.14 \mu\text{m}$. The Ginzburg-Landau parameter κ is therefore found to be²⁸

$$\kappa = \frac{\lambda(0)}{\xi} = \frac{0.37 \mu\text{m}}{0.14 \mu\text{m}} \approx 2.6 .$$

This value of κ is small and close to the border-line ($\kappa = \frac{1}{\sqrt{2}}$) between Type-I and Type-II superconductivity. If the mean free path l could be made larger by improving the quality of the sample, OsB_2 has the potential to be a non-elemental Type-I superconductor.

IV. CONCLUSION

We have synthesized the compounds OsB_2 and RuB_2 and measured their magnetic, transport and thermal properties. Our measurements confirm that OsB_2 undergoes a bulk transition into the superconducting state below 2.1 K . Analysis of our data suggests that OsB_2 is a moderate-coupling ($\lambda_{\text{ep}} = 0.4$ to 0.5) Type-II superconductor with a small Ginzburg-Landau parameter $\kappa \approx 2.6$ and an upper critical field $H_{\text{c}2}(0.5 \text{ K}) \sim 420 \text{ Oe}$. The temperature dependence of the superfluid density $n_s(T)$ is clearly consistent with an s -wave superconductor with a slightly enhanced gap $\Delta(0) = 1.90(5) \text{ K}_\text{B}T_\text{c}$ and a zero temperature London penetration depth $\lambda(0) = 0.37 \mu\text{m}$. In the normal state OsB_2 and RuB_2 are Pauli paramagnetic metals with very similar properties: residual resistivity $\rho_0 = 1.7(2)$ and $1.1(1) \mu\Omega \text{ cm}$; Pauli susceptibility $\chi_\text{P} = 3.4(5) \times 10^{-5}$ and $5.22(7) \times 10^{-5} \text{ cm}^3/\text{mol}$; electronic specific heat coefficient $\gamma = 1.90(1)$ and $1.72(3) \text{ mJ/mol K}^2$; low temperature T^3 lattice specific heat coefficient $\beta = 0.031(2)$ and $0.015(1) \text{ mJ/mol K}^4$; and density of states at the Fermi energy $N(\epsilon_\text{F}) = 2.21(9)$ and $3.0(2) \text{ states/(eV f.u.)}$ for OsB_2 and RuB_2 , respectively. To investigate the effect of boron off-stoichiometry on the superconducting properties of OsB_2 we also investigated samples with starting compositions $\text{OsB}_{1.9}$ and $\text{OsB}_{2.1}$. Both samples had a transition temperature $T_\text{c} = 2.1 \text{ K}$ indicating no significant dependence of T_c on the boron stoichiometry.

Acknowledgments

Ames Laboratory is operated for the U.S. Department of Energy by Iowa State University under Contract No. W-7405-Eng-82. This work was supported by the Director for Energy Research, Office of Basic Energy Sciences. R.P. also acknowledges support from NSF Grant number DMR-05-53285 and from the Alfred P. Sloan Foundation.

¹ J. Nagamatsu, N. Nakagawa, T. Muranaka, Y. Zenitani, and J. Akimitsu, *Nature* **410**, 63 (2001).

² D. Kaczorowski, A. J. Zaleski, O. J. Zogal, and J. Klamut,

cond-mat/0103571.

³ V. A. Gasparov, N. S. Sidorov, I. I. Zverkova, and M. P. Kulakov, JETP Lett. **73**, 532 (2001).

⁴ H. Rosner, W. E. Pickett, S.-L. Drechsler, A. Handstein, G. Behr, G. Fuchs, K. Nenkov, K.-H. Muller, and H. Eschrig, Phys. Rev. B **64**, 144516 (2001).

⁵ A. S. Cooper, E. Corenzwit, L. D. Longinotti, B. T. Matthias, and W. H. Zachariasen, Proc. Nat. Acad. Sci. USA **67**, 313 (1970).

⁶ N. I. Medvedeva, A. L. Ivanovskii, J. E. Medvedeva, and A. J. Freeman, Phys. Rev. B **64**, 020502(R) (2001).

⁷ J. M. Vandenberg, B. T. Matthias, E. Corenzwit, and H. Barz, Mater. Res. Bull. **10**, 889 (1975).

⁸ R. W. Cumberland, M. B. Weinberger, J. J. Gilman, S. M. Clark, S. H. Tolbert, and R. B. Kaner, J. Am. Chem. Soc., **127**, 7264 (2005).

⁹ M. Hebbachea, L. Stuparevi, and D. Zivkovi, Solid State Commun. **139**, 227 (2006).

¹⁰ Z. Y. Chen, H. J. Xiang, J. Yang, J. G. Hou, and Q. Zhu, Phys. Rev. B **74**, 12102 (2006).

¹¹ L. Stuparevic and D. Zivkovic, J. Therm. Anal. and Calor. **76**, 975 (2004).

¹² For a topical review see R. Prozorov and R. W. Giannetta, Supercond. Sci. Technol. **19**, R41 (2006).

¹³ R. Prozorov, R. W. Giannetta, A. Carrington, P. Fournier, R. L. Greene, P. Guptasarma, D. G. Hinks, and A. R. Banks, Appl. Phys. Lett. **77**, 4202 (2000).

¹⁴ R. Prozorov, R. W. Giannetta, A. Carrington, and F. M. Araujo-Moreira, Phys. Rev. B **62**, 115 (2000).

¹⁵ Rietveld analysis program DBWS-9807a release 27.02.99, ©1998 by R. A. Young, an upgrade of “DBWS-9411 - an upgrade of the DBWS programs for Rietveld Refinement with PC and mainframe computers, R.A. Young, J. Appl. Cryst. **28**, 366 (1995)”.

¹⁶ R. B. Roof Jr. and C. P. Kempler, J. Chem. Phys. **37**, 1473 (1962).

¹⁷ R. E. Peierls, *Quantum Theory of Solids* (Clarendon Press, Oxford, 1955).

¹⁸ R. D. Shannon, Acta. Cryst. **A32**, 751 (1976).

¹⁹ S. Chiodo, H. J. Gotsis, N. Russo, and E. Sicilia, Chem. Phys. Lett. **425**, 311 (2006).

²⁰ L. B. Mendelsohn and F. Biggs, Phys. Rev. A **2**, 1130 (1970).

²¹ C. Kittel, *Solid State Physics* (John Wiley and Sons, Inc., New York, 1966).

²² W. L. McMillan, Phys. Rev. **167**, 331 (1967).

²³ W. E. Pickett, Braz. J. Phys. **33**, 695 (2003).

²⁴ Z. X. Shi, M. Tokunaga, T. Tamegai, Y. Takano, K. Togano, H. Kito, and H. Ihara, Phys. Rev. B **68**, 104513 (2003).

²⁵ C. J. Gorter and H. Casimir, Physica **1**, 306 (1934).

²⁶ B. S. Chandrasekhar and D. Einzel, Ann. der Physik **2**, 535 (1993).

²⁷ R. Prozorov, T. A. Olheiser, R. W. Giannetta, K. Uozato, and T. Tamegai Phys. Rev. B. **73**, 184523 (2006).

²⁸ J. B. Ketterson and S. N. Song, *Superconductivity* (Cambridge University Press, United Kingdom, 1999).